ICC
Iranian Chemical Communication
Original Research Article
Payame Noor University http://icc.journals.pnu.ac.ir

$Fe_2V_4O_{13}$ assisted hetero-Fenton mineralization of methyl orange under UV-A light irradiation

Kaliyamoorthy Gowthami[a], Palusamy Suppuraj[a], Ganesamoorthy Thirunarayanan[a], Balu Krishnakumar[b], Abílio José Fraga do Nascimento Sobral[b], Meenakshisundaram Swaminathan[c], Inbasekaran Muthuvel[a,d]*

[a]*Department of Chemistry, Annamalai University, Annamalainagar 608 002, Tamil Nadu, India*

[b]*Department of Chemistry, University of Coimbra, Coimbra 3004-535, Portugal*

[c]*Nanomaterials Laboratory, International Research Centre, Kalasalingam University, Krishnan Koil 626 126, Tamil Nadu, India*

[d]*Department of Chemistry, M.R.Govt. Arts College, Mannargudi 614 001, Tamil Nadu, India*

Received: ……., Accepted: ……., Published: ……

Abstract

$Fe_2V_4O_{13}$ is prepared and characterized by X-ray diffraction (XRD), Fourier transform infrared (FT-IR), UV-diffuse reflectance spectroscopy (UV-DRS), high resolution scanning electron microscopy (HR-SEM) using energy dispersive X-ray spectroscopy (EDX) analysis. The hetero-Fenton catalyst can be used to mineralize Methyl Orange (MO) under UV-A light. The mineralization rate is influenced by hydrogen peroxide (H_2O_2) concentration, pH, and catalyst loading. The reusability of $Fe_2V_4O_{13}$ is analyzed by five successive runs. At the maximum, 95% of degradation is observed in all five cycles. Therefore, the $Fe_2V_4O_{13}$ catalyst is found to be reusable. The mineralization is confirmed by chemical oxygen demand (COD) measurements. Mechanism of the heterophoto-Fenton process is also proposed.

Keywords: $Fe_2V_4O_{13}$; methyl orange; wastewater treatment; hetero-Fenton reaction; photocatalysis.

Introduction

Environmental pollution by dye wastewater is the most serious issue in the developing countries. Using the common treatment methods, it is very difficult to degrade dyes that have a complex aromatic structure as they produce toxic and carcinogenic by-products from various reactions such as hydrolysis and oxidation in aqueous media. So from the point of view for the public health and safety, these by-products should be removed using suitable treatment methods [1-6]. Advanced oxidation processes are used to degrade any pollutants in aqueous media using strong oxidants, e.g., hydroxyl radicals ($HO^{\bullet}$). Fenton reaction [7] produces hydroxyl radicals. However, the homogeneous Fenton reaction has some disadvantages: i) reaction can be carried out only in a short range of pH and ii) formation of iron sludge at the end of the process. The heterogeneous Fenton type catalysts are prepared using various

*Corresponding author: Inbasekaran Muthuvel
Tel: +91 (04367-255440), Fax: +91 (9940594367)
E-mail: profmuthuvelchem@yahoo.com

supports such as metal oxides, graphite, Al_2O_3, bentonite, monmorillonite K10, fire clay, and so on. The advantages of hetero-Fenton type catalyst are: i) a wide pH range of catalyst, ii) reusability, and iii) no sludge formation [8-13]. Similarly, iron-containing material, such as $Fe_{3-x}Cr_xO_4$ shows higher photocatalytic activity due to the more efficient regeneration of the Fenton-active species Fe^{2+} by coupling redox pairs Fe^{3+}/Fe^{2+} and Cr^{3+}/Cr^{2+} [14]. Iron and copper pyrovanadate are reported to be cost effective, recyclable, stable heterogeneous Fenton catalysts for mineralization of toxic organics [14,15]. Complex Fe vanadates have attracted growing interest in energy applications.

Their V–O polyhedral linkages are effective for catalytic, electrochemical, and ion-conducting properties [16,17]. Recently, $Fe_2V_4O_{13}$ nanoribbon (NR)/reduced graphene oxide (RGO)/CdS nanoparticle grown on the stainless-steel mesh which is rationally designed for photoconversion of gaseous CO_2 into renewable hydrocarbon fuels such as CH_4 [18]. $Fe_2V_4O_{13}$ has also been used to degrade organic pollutants as it has special two-way Fenton-like mechanism and synergistic activation of Fe and V [19,20]. $Fe_2V_4O_{13}$ has also been investigated for visible-light photoreduction of CO_2 [21].

In this current study, we have prepared the $Fe_2V_4O_{13}$ novel vanadates (iron tetrapolyvanadate) using the simple liquid-phase precipitation method. The prepared $Fe_2V_4O_{13}$ multicomponent system shows great potential for the efficient mineralization of MO under UV-A light irradiation.

Experimental

Synthesis of $Fe_2V_4O_{13}$

The heterogeneous Fenton-like catalyst $Fe_2V_4O_{13}$ is prepared using the simple liquid-phase precipitation method (SLPP). Ferric nitrate aqueous solution (0.1 M) is quickly poured into an aqueous solution NH_4VO_3 (0.2 M). Under continuous stirring at 80 °C, a yellow precipitate is formed; and on further stirring for 3 h, the color of the precipitate has been changed to brown. The precipitate is then isolated by filtration, washed several times with distilled water and ethanol, and dried at 100 °C in 1 h. Finally, it is calcined in muffle furnace at 500 °C for 6 h to get $Fe_2V_4O_{13}$.

Photoreactor

Heber multilamp photoreactor model HML-MP 88 (Figure 1) is used for photodegradation experiments with UV light. This model consists of eight medium pressure mercury vapour lamps of 8 W, set in parallel, emitting 365 nm wavelength. It has a reaction chamber with specially designed reflectors made of highly polished aluminium and built in cooling fan at the bottom. It is provided with magnetic stirrer at the center. Open borosilicate glass tube of 40 cm height and 12.6 mm diameter is used as a reaction vessel with the total radiation exposure length of 330 mm. The irradiation is carried out using four parallel 8 W medium pressure mercury lamps in open-air condition. The light intensity is measured using ferrioxalate actinometer [22] and it is found to be 1.381×10^{-6} einstein L^{-1} s^{-1}.

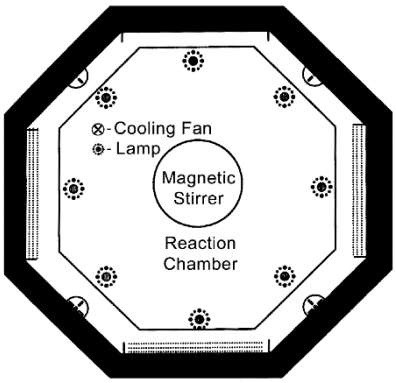

Figure 1. Schematic diagram of photoreactor

Photocatalytic degradation experiments

In all experiments, 50 mL of the dye solution containing an appropriate quantity of $Fe_2V_4O_{13}$, H_2O_2 is used. The suspension is stirred for 30 min in dark and then it is irradiated. The solution and dye are continuously aerated by a pump to provide oxygen as well as to mix reaction medium completely. At a specific time interval, 2–3 mL of the sample is withdrawn and centrifuged to separate the catalyst. One milliliter of the centrifugate is diluted to 10 mL and its absorbance is measured at 464 nm using UV-Vis spectrophotometer to determine the dye concentration. From this, the percentage of degraded dye is determined.

The photocatalytic degradation of MO containing $Fe_2V_4O_{13}$ catalyst obeys *pseudo*-first order kinetics. At low initial dye concentration, the rate expression is given in the following equation:

$$d[C]/dt = k'[C] \quad (1)$$

where k' is the *pseudo*-first order rate constant. The dye is adsorbed onto the catalyst surface and adsorption-desorption equilibrium is reached in 10 min. After adsorption, the equilibrium concentration of the dye solution is determined and it is taken as the initial dye concentration for kinetic analysis. Integrating eqn. 1 (with the limit of $C = C_0$ at $t = 0$ with C_0 being the equilibrium concentration of the bulk solution) gives eqn. 2.

$$\ln (C_0/C) = k't \quad (2)$$

where C_0 is the equilibrium of dye concentration and C is the concentration at time t. *Pseudo*-first order rate constant k' is determined from the plot of $\ln C_0/C$ *Vs* t.

Characterization techniques

Fourier transform-infrared spectra are recorded using Thermo Nicolet iS5 FT-IR spectrometer in KBr pellet. High resolution scanning X-ray diffraction spectra are recorded on the Equinox-1000 model X-ray diffractometer from analytical instruments operated at 30 kV and 30 mA with CuKα (1.54056 Å) radiation. HR-SEM images are taken using FEI quanta FEG 250 high resolution scanning electron microscope (the Netherlands). Samples are mounted on a gold platform placed in the scanning electron microscope for taking images at various magnifications. EDX is performed at various points of the surface in order to minimize any possible anomalies arising from the heterogeneous nature of the analyzed surface. COD is determined by a reported procedure [23].

Results and discussion

FT-IR

The FT-IR spectrum of $Fe_2V_4O_{13}$ is shown in Figure 2, and the band at 1028 cm^{-1} is assigned to V–O terminal stretching vibrations and the characteristic absorption band at 711 cm^{-1} correspond to the V–O–Fe stretching mode. The absorption band at 510cm^{-1} is assigned to Fe–O stretching mode [21].

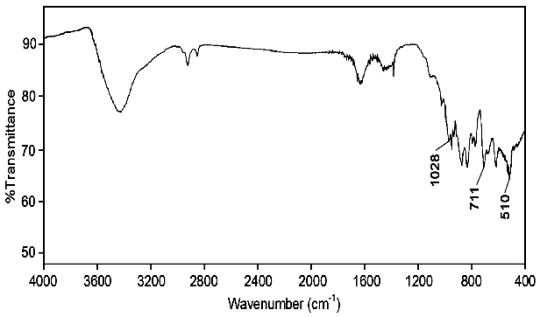

Figure 2. FT-IR spectrum of $Fe_2V_4O_{13}$

XRD

The XRD patterns of the prepared materials are shown in Figure 3. The XRD pattern of the $Fe_2V_4O_{13}$ catalyst dried at 100 °C shows a weak peak at the 2θ angle of about 25°, suggesting that the solid catalyst is a kind of amorphous compound [24]. At 500 °C, the catalyst has three intense diffraction peaks at the 2θ angles of 12.5, 22.7, and 26.7°. The diffraction peaks are well matched to the monoclinic phase of $Fe_2V_4O_{13}$ (JCPDS No. 00-039-0893). The strong and narrow diffraction peaks demonstrated good crystallinity.

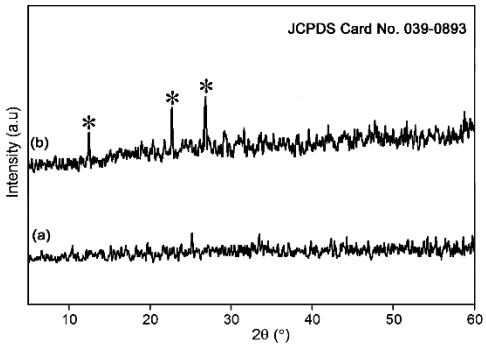

Figure 3. XRD patterns of $Fe_2V_4O_{13}$: a) 100 °C and b) 500 °C

UV-DRS

The absorbance spectrum illustrates that the absorption edge of $Fe_2V_4O_{13}$ extends to the visible region (around 580 nm) and also suggests the possibility of photoactivity of this material under visible light also (Figure 4). Kubelka-Munk plots for $Fe_2V_4O_{13}$ are shown in insets of Figure 4. The optical band gap of $Fe_2V_4O_{13}$ is calculated to be 2.21 eV from the Tauc plot, $(\alpha h\nu)^2$ $(eV/cm)^2$ Vs $h\nu$ (eV).

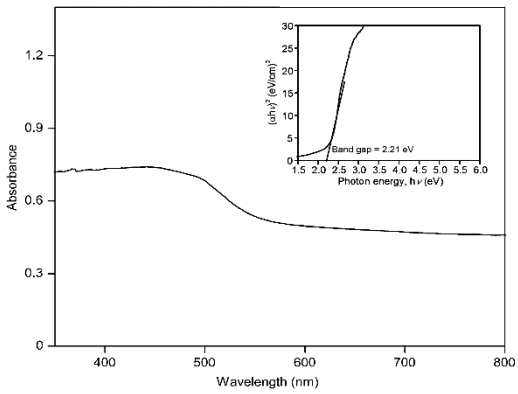

Figure 4. DRS of $Fe_2V_4O_{13}$. Inset shows the plot of $(\alpha h\nu)^2$ $(eV/cm)^2$ *Vs* $h\nu$ (eV) for determining band gap energy of $Fe_2V_4O_{13}$

HR-SEM with EDX

Figure 5 shows the HR-SEM images of $Fe_2V_4O_{13}$. HR-SEM images showed a flaky structure in all images; however, aggregation (or) interconnection appeared when $Fe_2V_4O_{13}$ is thermally heated at 500 °C for 6 h. The corresponding energy-dispersive X-ray (EDX) spectrum demonstrates the presence of Fe, V, and O in the $Fe_2V_4O_{13}$ catalyst (Figure 6).

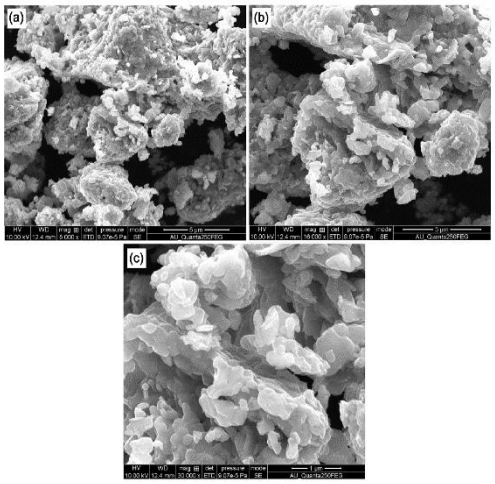

Figure 5. HR-SEM images of $Fe_2V_4O_{13}$: a) 5 µm, b) 3 µm and c) 1 µm

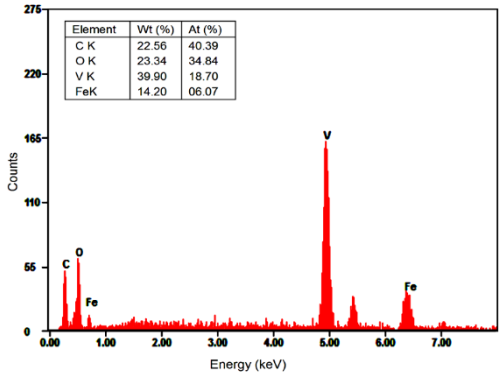

Figure 6. EDX of $Fe_2V_4O_{13}$

Photocatalytic activity of $Fe_2V_4O_{13}$

Primary analysis

The photocatalytic activity of $Fe_2V_4O_{13}$ is evaluated by degradating MO under UV light. Controlled experiments under various reaction conditions are carried out and the results are shown in Figure 7. From the results, it is evident that the dye is resistant to direct photolysis by UV-A light (curve a). In the presence of dye/H_2O_2/dark, a 11% decrease in the dye concentration at the time to 60 min (curve b) is observed. There is no appreciable decrease in the dye concentration when it is treated with $Fe_2V_4O_{13}$/dark (curve c). The dye on irradiation with heterophoto-Fenton like catalyst $Fe_2V_4O_{13}$ with H_2O_2 undergoes 95% degradation in 50 min (curve d). There is a small decrease (28%) in the dye concentration when it is treated with dye/$Fe_2V_4O_{13}$/H_2O_2/dark (curve e). To compare the heterogeneous-Fenton reaction with that of the homogeneous system, we have taken the same amount of Fe^{3+} present in heterophoto-Fenton catalyst ($Fe_2V_4O_{13}$) and carried them out in the homogeneous photo-Fenton reaction (curve f). In the first 20 min, the reaction is fast in the homogeneous Fenton process and a sharp decrease of MO concentration is observed. After 20 min, the dye removal was occurred gradually.

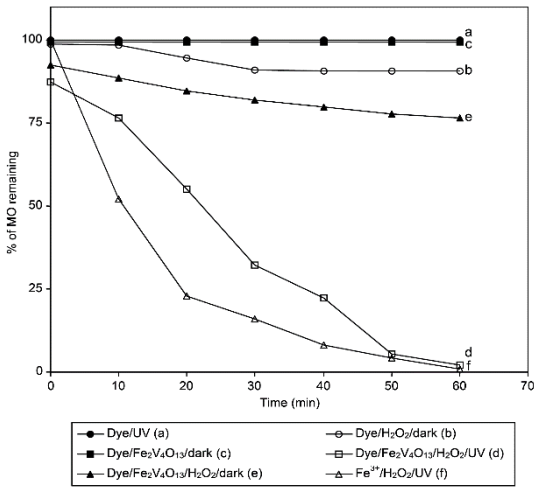

Figure 7. Primary analysis of MO under UV light. [MO] = 4×10^{-4} M, catalyst suspended = 0.600 g L^{-1}, H_2O_2 = 10 mmol, airflow rate = 8.1 mL s^{-1}, pH = 6.0, $I_0 = 1.381 \times 10^{-6}$ einstein L^{-1} s^{-1}

In the homogeneous process, the free Fe^{3+} ions in solution are active, and initially they react very quickly; however, the rate decreases after 20 min. This decrease may be due to the decrease in the H_2O_2 concentration in solution after 20 min. But in the heterogeneous process, the photoreductions of Fe^{3+} to Fe^{2+}, V^{5+} to V^{4+} followed by the reaction between Fe^{2+} with H_2O_2, and V^{4+} with H_2O_2 take place at the surface of $Fe_2V_4O_{13}$, generating highly oxidative $^{\bullet}OH$ radicals. Meanwhile, H_2O_2 itself produces limited number of $^{\bullet}OH$ radicals with UV light. These $^{\bullet}OH$ radicals attack dye molecules leading to reaction intermediates that are finally mineralized into CO_2 and H_2O. The release of $^{\bullet}OH$ radicals to the solution from $Fe_2V_4O_{13}$ catalyst is gradual and the time required for 98% degradation is 60 min, whereas mineralization is almost complete in 60 min for the homogeneous process. But the heterogeneous photo-Fenton catalyst has

the advantages of easy removal and reusability.

Influence of process parameters on photodegradation of MO with $Fe_2V_4O_{13}$ catalyst

Effect of catalyst loading

The effect of catalyst weight on the percentage removal of MO is investigated from 0.200 to 0.800 g L^{-1} of catalyst. The results are shown in Figure 8. Adding catalyst from 0.200 to 0.600 g L^{-1} increases the MO removal rate sharply from 0.0024 to 0.0287 min^{-1}. When the catalyst weight is above 0.600 g L^{-1}, the removal rate decreases.

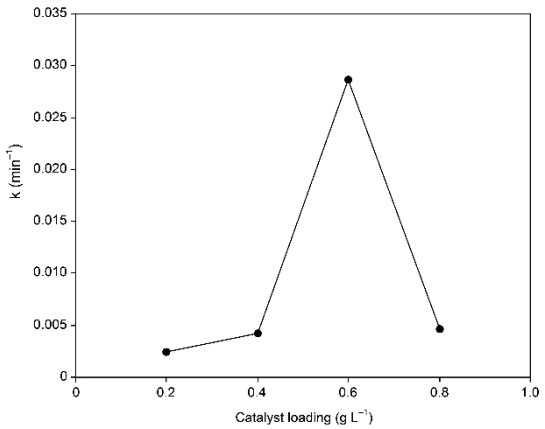

Figure 8. Effect of catalyst loading. [MO] = 4×10^{-4} M, H_2O_2 = 10 mmol, airflow rate = 8.1 mL s^{-1}, pH = 6.0, $I_0 = 1.381 \times 10^{-6}$ einstein L^{-1} s^{-1}

The enhancement of removal rate is due to i) the increase in the amount of catalyst weight, which increases the number of dye molecules adsorbed and ii) the increase in the density of particles in the area of illumination. Above 0.600 g L^{-1} of catalyst, the removal rate is decreased. This may be due to the enhancement of light reflectance by the catalyst and the decrease in light penetration [25]. Thus, the optimum amount of catalyst concentration is found to be 0.600 g L^{-1} (30 mg/50 mL) and is used as the catalyst dosage for the photocatalytic reactions.

Effect of initial solution pH

Dye wastewater is discharged at different pH levels. Therefore, it is important to study the role of pH on degradation efficiency. Experiments are carried out at various pH levels, ranging from 4 to 9 with a constant amount of dye (4×10^{-4} M) and catalyst (0.600 g L^{-1}). Figure 9 illustrates the increase in the degradation from 73 to 98% for the increase of pH from 4 to 6 (60 min). Further increase of pH above 6 decreases the degradation efficiency. The maximum MO degradation is observed at pH 6. Hence, pH 6 is optimum for this heterogeneous photo-Fenton MO degradation, which overcomes the drawback of a narrow pH range of homogeneous Fenton. Above pH 6, the catalyst activity decreases.

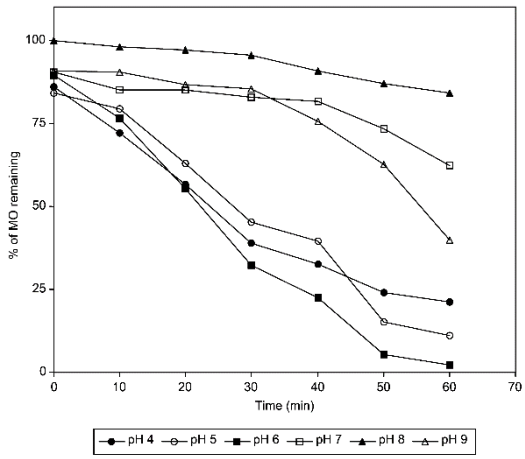

Figure 9. Effect of initial solution pH. [MO] = 4×10^{-4} M, catalyst suspended = 0.600 g L^{-1}, H_2O_2 = 10 mmol, airflow rate = 8.1 mL s^{-1}, I_0 = 1.381×10^{-6} einstein L^{-1} s^{-1}

Effect of H_2O_2 dosage

The MO degradation with $Fe_2V_4O_{13}$ at pH 6 at various H_2O_2 concentrations is studied. Adding H_2O_2 (6–10 mmol) increases the *pseudo*-first order rate constant from 0.0287 to 0.0377 min^{-1} in the MO mineralization (Figure 10). Further increase of H_2O_2 above 10 mmol decreases the MO mineralization rate (30 min). Hence, 10 mmol of H_2O_2 is the optimum level for the MO mineralization.

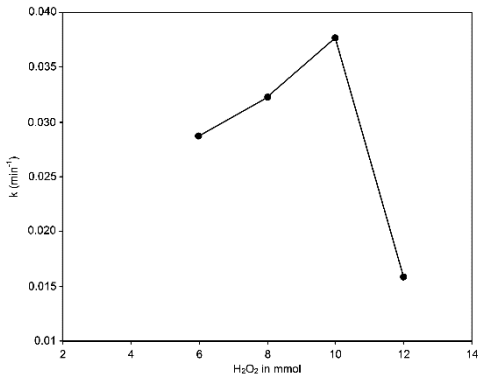

Figure 10. Effect of H_2O_2 dosage. [MO] = 4×10^{-4} M, catalyst suspended = 0.600 g L^{-1}, airflow rate = 8.1 mL s^{-1}, pH = 6.0, I_0 = 1.381×10^{-6} einstein L^{-1} s^{-1}, irradiation time = 30 min

The enhancement of mineralization by adding H_2O_2 is due to the increased production of hydroxyl radicals (eqns. 3 and 4).

$$H_2O_2 + h\nu\,(\lambda<380\text{ nm}) \rightarrow 2\ OH^{\bullet} \quad (3)$$

$$H_2O_2 + O_2^{\bullet-} \rightarrow {}^{\bullet}OH + OH^- + O_2 \quad (4)$$

At H_2O_2 dosage above 10 mmol, the decrease in removal rate is due to hydroxyl radicals and the hole scavenging effect of H_2O_2 (eqns. 5 and 6) [26].

$$H_2O_2 + {}^{\bullet}OH \rightarrow HO_2^{\bullet} + H_2O \quad (5)$$

$$HO_2^{\bullet} + {}^{\bullet}OH \rightarrow H_2O + O_2 \quad (6)$$

Effect of initial dye concentration

Many researchers have investigated the effect of initial dye concentration on the mineralization in solution. Increasing the initial dye concentration from 1 to 5×10^{-4} M decreases the degradation rate constant from 0.084 to 0.013 min^{-1} in 20 min (Figure 11). The degradation rate relates to the $^{\bullet}OH$ (hydroxyl radical) formation on catalyst surface and the

probability of •OH reacts with dye molecules. For all initial dye concentrations, the catalyst amount and light intensity are same. Since generating hydroxyl radical remains constant, the probability of dye molecule to react with hydroxyl radical decreases [27]. At high initial dye concentrations, the path length of the photon entering into the solution also decreases. However, it should be pointed out that even at a high initial concentration of MO (5×10^{-4} M), about 70% of dye removal is achieved in 60 min. This indicates that $Fe_2V_4O_{13}$ catalyst can also work well at high initial MO concentrations.

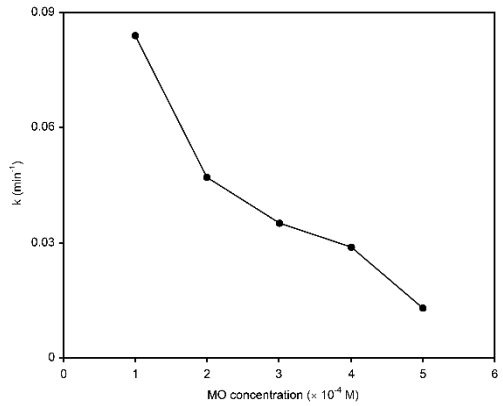

Figure 11. Effect of initial dye concentration. Catalyst suspended = 0.600 g L^{-1}, H_2O_2 = 10 mmol, airflow rate = 8.1 mL s^{-1}, pH = 6.0, I_0 = 1.381 × 10^{-6} einstein L^{-1} s^{-1}, irradiation time = 20 min

Long-term stability

The reusability of the heterogeneous photo-Fenton catalyst is tested and the results are shown in Figure 12. About 98% dye removal takes place at 60 min in the first run.

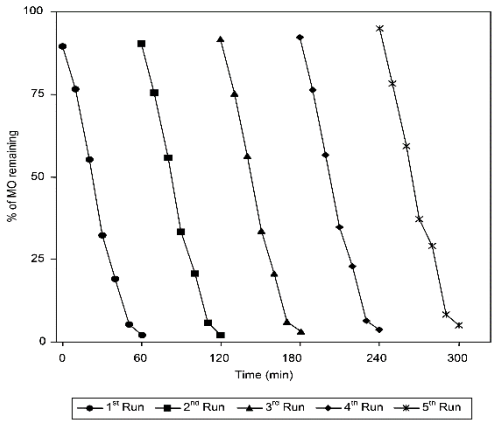

Figure 12. Effect of long-term stability. [MO] = 4 × 10^{-4}M, catalyst suspended= 0.600 g L^{-1}, H_2O_2= 10 mmol, airflow rate= 8.1 mL s^{-1}, pH = 6.0, I_0 = 1.381 × 10^{-6} einstein L^{-1} s^{-1}

The same catalyst is separated, dried, and used again. In the second run, 98% of dye is removed at 60 min. Third run gave 97% dye removal at 60 min. Fourth run gave 97% dye removal and fifth run gave 97% dye removal. There is no significant decrease in degradation even at fifth run. So, the catalyst is reusable.

Mechanism

On the basis of the above experimental observations and corroborating with the existing

literature, a possible mechanism has been proposed for the degradation of Methyl Orange dye in the presence of iron polyvanadate, H_2O_2, and UV-A light. V(V) and Fe(III) may simultaneously activate H_2O_2 to give $^{\bullet}OH$ radicals (Scheme 1).

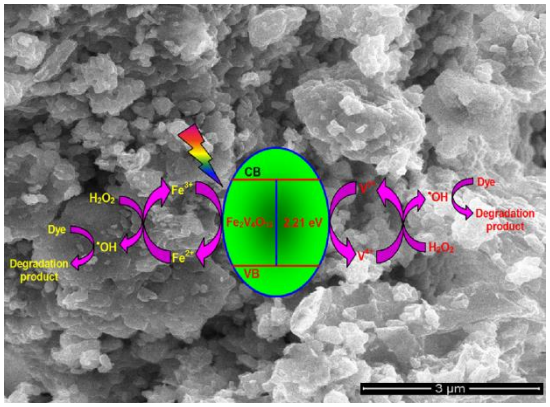

Scheme 1. Mechanism of degradation of MO by $Fe_2V_4O_{13}$ in the presence of H_2O_2 and UV light

$$\equiv Fe^{3+} + H_2O_2 \xrightarrow{h\nu} Fe^{2+} + HOO^{\bullet} + H^+ \quad (7)$$

$$\equiv Fe^{2+} + H_2O_2 \xrightarrow{h\nu} Fe^{3+} + OH^{\bullet} + HO^- \quad (8)$$

$$\equiv V^{5+} + H_2O_2 \xrightarrow{h\nu} V^{4+} + {}^{\bullet}OOH + H^+ \quad (9)$$

$$\equiv V^{4+} + H_2O_2 \xrightarrow{h\nu} V^{5+} + OH^- + {}^{\bullet}OH \quad (10)$$

The high catalytic activity of $Fe_2V_4O_{13}$ could partly contribute to the two-way catalytic mechanism involved in the Fe(III)/Fe(II) and V(V)/V(IV) redox couples [14].

Generally, in heterogeneous Fenton-like catalysts, a Lewis acid, which is associated with iron could facilitate the reduction of the ferric ion by H_2O_2 attracting the electron density from the iron center. The facilitation will accelerate the whole Fenton-like reaction as the reduction of ferric ion is the dominant rate step of Fenton-like reaction. In $Fe_2V_4O_{13}$, V(V) has many positive charges and is a strong Lewis acid. Hence, V(V) can facilitate the reduction of Fe(III), sequentially leading to the enhancement of the overall MO degradation rate.

The active free radicals generated in the cycles of iron and vanadate ions can oxidize most of the organic pollutants in wastewater to carbon dioxide, water, and other inorganic compounds (eqn. 11).

$$^{\bullet}OH + MO \rightarrow CO_2 + H_2O + SO_4^- + NO_3^- \quad (11)$$

COD measurements

As the reduction of chemical oxygen demand (COD) reflects the extent of degradation or mineralization of an organic species, the percentage change in COD is studied for dye sample (initial concentration 4×10^{-4} M) under optimum conditions. The percentage of COD reduction is 70% in 60 min irradiation for MO degradation with $Fe_2V_4O_{13}$. About 80% degradation is observed with $Fe_2V_4O_{13}$ in 40 min irradiation by absorbance measurements, whereas only 70% mineralization is observed in 60 min by COD measurements under the same condition. This reveals the presence non-absorbing organic intermediates at the time of 60 min. Hence, complete mineralization may be achieved at the time of 90 min irradiation.

Conclusion

Heterogeneous Fenton-like $Fe_2V_4O_{13}$ catalyst is prepared and it is calcined at

500 °C. It is used as photocatalyst for the degradation of Methyl Orange (MO) under UV light. The prepared $Fe_2V_4O_{13}$ is characterized by XRD, FT-IR, UV-DRS, and HR-SEM with EDX. $Fe_2V_4O_{13}$ is found to be an effective catalyst for the MO mineralization using H_2O_2 as oxidant possibly by Fe and V-based two-way Fenton-like mechanism. The prepared $Fe_2V_4O_{13}$ is characterized by photocatalytic activity of MO dye used as a pollutant. Almost 95% mineralization is observed at 60 min. In the $Fe_2V_4O_{13}$ catalyst, Fe and V-based two-way Fenton-like mechanism is operated as they speed up the reaction faster when compared to ordinary Fenton and heterogeneous Fenton-type reaction. This catalyst is reusable for multiple run. Hence, the catalyst can be a viable industrial wastewater treatment method for short duration.

Acknowledgments

One of the authors (I. Muthuvel) would like to thank the University Grants Commission (UGC), New Delhi, for their financial support for through research Grant No. UGC sanctioned letter F.No-43-222/2014(SR). This work is supported by FCT/QREN-COMPETE through the project PTDC/AAC-CLI/118092/2010 and grant SFRH/BPD/86971/2012 (B. Krishnakumar).

References

[1] N.M. Mahmoodi, *Mater. Res. Bull.*, **2013**, 48, 4255–4260.

[2] Z. Zainal, L.K. Hui, M.Z.O. Hussein, A.H. Abdullah, I.R. Hamadneh, *J. Hazard. Mater.*, **2009**, *164*, 138–145.

[3] A. Ozcan, A.S. Ozcan, *J. Hazard. Mater.*, **2005**, *125*, 252–259.

[4] V.P. Santos, M.F.R. Pereira, P.C.C. Faria, J.J.M. Orfao, *J. Hazard. Mater.*, **2009**, *162*, 736–742.

[5] N.M. Mahmoodi, F. Najafi, *Mater. Res. Bull.*, **2012**, *47*, 1800–1809.

[6] N.M. Mahmoodi, F. Najafi, *Micropor. Mesopor. Mater.*, **2012**, *156*, 153–160.

[7] M.B. Kasiri, H. Aleboyeh, A. Aleboyeh, *Appl. Catal. B*, **2008**, *84*, 9–15.

[8] I. Muthuvel, B. Krishnakumar, M. Swaminathan, *Indian J. Chem.*, **2014**, *53A*, 672–678.

[9] I. Muthuvel, B. Krishnakumar, M. Swaminathan, *Indian J. Chem.*, **2012**, *51A*, 807–811.

[10] I. Muthuvel, B. Krishnakumar, M. Swaminathan, *J. Environ. Sci.*, **2012**, *24*, 529–535.

[11] I. Muthuvel, M. Swaminathan, *Sol. Energy Mater. Sol. Cells*, **2008**, *92*, 857–863.

[12] N.M. Mahmoodi, *J. Mol. Catal. A*, **2013**, *366*, 254–260.

[13] T.A. Kurniawan, W.H. Lo, *Water Res.*, **2009**, *43*, 4079–4091.

[14] Y.Y. Zhang, J.H. Deng, C. He, S.S. Huang, S.H. Tian, Y. Xiong, *Environ. Technol.*, **2010**, *31*, 145–154.

[15] K. Sangeeta, C.N.P. Singh, P. Arpita, A. Rakshit, P.P. Bala, *Indian J. Chem.*, **2015**, *54A*, 1057–1061.

[16] L.Q. Mai, L. Xu, Q. Gao, C. Han, B. Hu, Y. Pi, *Nano Lett.*, **2010**, *10*, 2604–2608.

[17] S.Y. Zhang, W.Y. Li, C.S. Li, J. Chen, *J. Phys. Chem. B*, **2006**, *110*, 24855–24863.

[18] P. Li, Y. Zhou, H. Li, Q. Xu, X. Meng, X. Wang, M. Xiao, Z. Zou, *Chem. Commun.*, **2015**, *51*, 800–803.

[19] Y.Y. Zhang, C. He, J.H. Deng, Y.T. Tu, J.K. Liu, Y. Xiong, *Res. Chem. Intermed.*, **2009**, *35*, 727–737.

[20] Y.Y. Zhang, J.H. Deng, C. He, S.S. Huang, S.H. Tian, Y. Xiong, *Environ. Technol.*, **2010**, *31*, 145–154.

[21] P. Li, Y. Zhou, W. Tu, Q. Liu, S. Yan, Z. Zou, *ChemPlusChem.*, **2013**, *78*, 274–278.
[22] H.J. Kuhn, S.E. Braslavsky, R. Schmidt, *Pure Appl. Chem.*, **2004**, *76*, 2105–2146.
[23] B. Subash, B. Krishnakumar, B. Sreedhar, M. Swaminathan, M. Shanthi, *Superlattices Microstruct.*, **2013**, *54*, 155–171.
[24] E. Baudrin, S. Denis, F. Orsini, L. Seguin, M. Touboul, J.M. Tarascon, *J. Mater. Chem.*, **1999**, *9*, 101–105.
[25] G. Thennarasu, A. Sivasamy, *J. Chem. Technol. Biotechnol.*, **2015**, *90*, 514–524.
[26] G.V. Buxton, C.L. Green Stock, W.P. Helman, A.B. Ross, *J. Phys. Chem. Ref. Data*, **1988**, *17*, 513–886.
[27] K. Velmurugan, B. Krishnakumar, B. Subash, M. Swaminathan, *Sol. Energy Mater. Sol. Cells*, **2013**, *108*, 205–212.